ELSEVIER

www.elsevier.nl/locate/jorganchem

Journal of Organometallic Chemistry 599 (2000) 62–68

Journal of Organometallic Chemistry

Synthesis, electrochemistry, Langmuir–Blodgett deposition and photophysics of metal-coordinated fullerene–porphyrin dyads

Tatiana Da Ros [a], Maurizio Prato* [a,1], Maurizio Carano [b], Paola Ceroni [b], Francesco Paolucci* [b,2], Sergio Roffia [b], Lodovico Valli* [c,3], DirkM. Guldi* [d,4]

[a] *Dipartimento di Scienze Farmaceutiche, Università di Trieste, Piazzale Europa 1, I-34127 Trieste, Italy*
[b] *Dipartimento di Chimica 'G. Ciamician', Università di Bologna, via Selmi 2, I-40126 Bologna, Italy*
[c] *Dipartimento di Ingegneria dell'Innovazione, Edificio 'La Stecca', via Monteroni, I-73100 Lecce, Italy*
[d] *Radiation Laboratory, University of Notre Dame, Notre Dame, IN 46656, USA*

Received 18 October 1999; received in revised form 8 December 1999

Abstract

A novel fullerene–Ru–porphyrin conjugate (**3b**) for Langmuir–Blodgett (LB) film deposition has been synthesized. The side polar chain that characterizes the complex is necessary to introduce enough amphiphilicity in these otherwise non-polar moieties. The complex can be deposited on solid substrates via the LB technique and the films obtained show charge separation upon light irradiation. In addition, a careful cyclic voltammetry study of the complex is reported.

Keywords: Fullerenes; Ruthenium; Porphyrin; Langmuir–Blodgett; Photophysics

1. Introduction

Recent contributions from three different laboratories reported that fullerene derivatives bearing a pyridine ring can form complexes with metalloporphyrins [1–3]. In particular, we have shown that electron and/or energy transfer occurs in these complexes upon light irradiation [3–5]. In order to check the suitability of these materials for any practical applications, such as optical limiting, photovoltaic devices, etc., their deposition and organized assemblies on solid, transparent substrates represent an important step [6,7].

In this paper, we report an electrochemical study of a fullerene–porphyrin conjugate, carried out in order to establish the redox properties of this class of donor–acceptor complexes. We then describe the preparation and Langmuir–Blodgett (LB) deposition of a suitably functionalized complex. Finally, the behavior of the deposited films upon light irradiation and the associated phenomena have been studied by transient absorption spectrophotometry.

2. Results and discussion

2.1. Synthesis and characterization

Fullerene–porphyrin conjugates (**3a**–**b**) were prepared according to Scheme 1 [8,9]. Whereas **3a** was synthesized as a model for electron-transfer studies in solution [4], **3b** was prepared for the purpose of LB film deposition, since we have already observed that fulleropyrrolidines functionalized at nitrogen with hydrophilic chains possessing the correct hydrophobic–hydrophilic balance to form strong monomolecular layers at the air–water interface [10]. The existence of a truly monolayered structure was confirmed by means of surface pressure (Π) versus surface area (A) isotherms. Also monolayers prepared from these amphiphilic fullerene derivatives were transferred successfully to quartz substrates, via repeated dipping of the substrate into the aqueous subphase and withdrawing from the latter [10].

[1] *Corresponding author. Fax: +39-40-52572; e-mail: prato@univ.trieste.it
[2] *Corresponding author.
[3] *Corresponding author.
[4] *Corresponding author.

0022-328X/00/$ - see front matter
PII: S0022-328X(99)00754-8

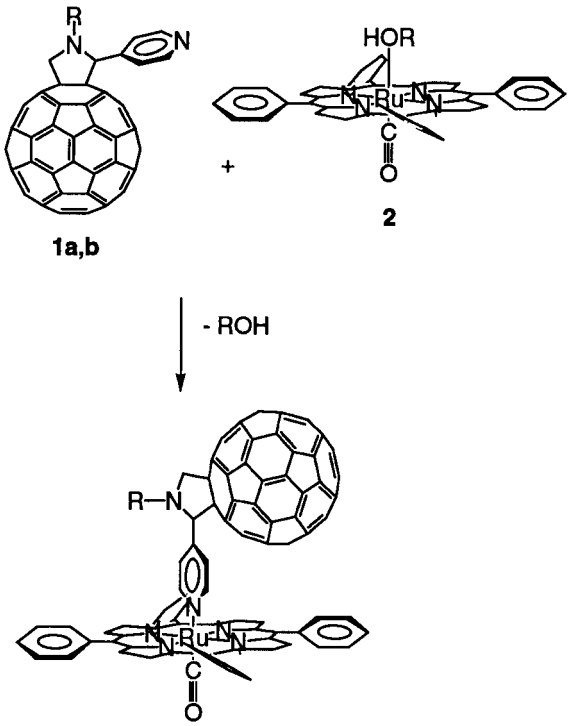

a, R = CH_3
b, R = $CH_2CH_2OCH_2CH_2OCH_2CH_2OCH_3$

Scheme 1.

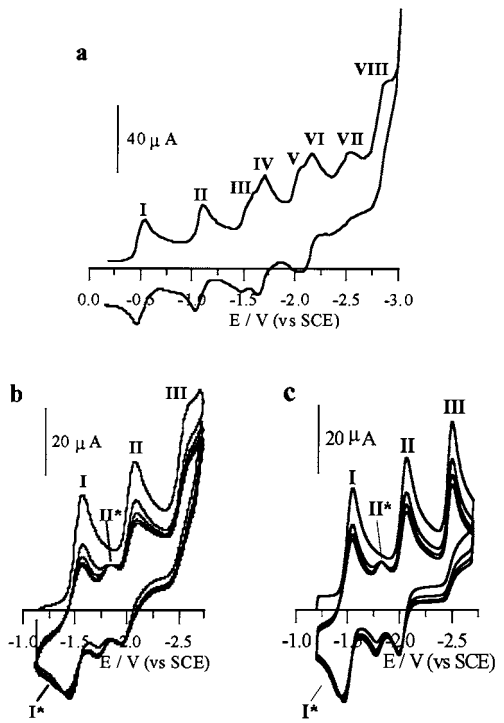

Fig. 1. CV curves at r.t. of a 0.4 mM TBAH–THF solution of (a) dyad **3a**, $v = 0.5$ V s^{-1} and (b) model **4**, $v = 1$ V s^{-1}. Working electrode: Pt wire (0.15 cm^2). (c) Digital simulation in the conditions of (b).

Fulleropyrrolidine (**1b**) was prepared as already reported [11]. The simple mixing of chloroform or methylene chloride solutions of **1b** and RuTPP (TPP = tetraphenylporphyrin) **2** instantaneously affords the replacement of the alcoholic moiety in **2** by the pyridine derivative **1b**. The reaction can be followed easily by ^{1}H-NMR. The two protons of the pyridine ring, upon Ru complexation, shift from 8.68 in **1b** to 1.58 ppm in **3b** ($CDCl_3$). The complex was also characterized by ^{13}C-NMR, UV–vis and electrospray-mass spectrometry (ES MS).

2.2. Electrochemistry

In order to obtain useful information on the redox properties of these complexes, **3a** was studied by cyclic voltammetry (CV), whereas **1a** and the RuTPP complex **4** were used as model compounds. The CV curve relative to a TBAH–THF solution of dyad **3a** at 25°C is shown in Fig. 1(a).

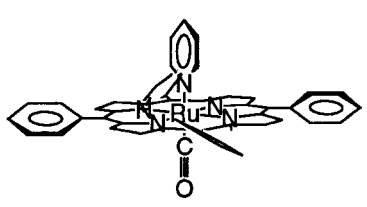

4

The cathodic CV pattern consists of eight one-electron reduction processes. All these electron transfers are reversible, with the last one being very close to the base solution discharge. Based on the analogous CV behavior of fulleropyrrolidine (**1a**), five out of these eight reductions can be ascribed to the fullerene-centered reduction. This assignment stems from the coincidence of their $E_{1/2}$ values (see Table 1) with peaks I, II, IV, VI and VIII. The remaining processes, namely, peaks III, V and VII, take place on the porphyrin moiety. The corresponding $E_{1/2}$ values compare very well with those of the porphyrin model (**4**). However, the comparison of the CV pattern of the two species exhibits a strikingly greater stability of the multiply-reduced porphyrin in **3a** than in the model compound **4**. Fig. 1(b) shows in fact that, upon cycling the potential repeatedly, two novel reduction peaks, I* and II* (the former is hidden under pristine peak I), develop. Experiments carried out upon varying the reversing potential showed that the occurrence of these peaks is associated with the third, only partially reversible, reduction. These results are in strong disagreement with the redox behavior of the porphyrin moiety in **3a**. Indication that the reaction is a second-order process with respect to **4** evolves from the observation that the CV pattern reveals a strong concentration dependence.

Table 1
Half-wave potentials ($E_{1/2}$ vs. SCE) for dyad **3a** and model compounds **4** and **1a** at 25°C in TBAH–THF solutions

Compound	$E_{1/2}$/V vs. SCE									
	A	B	I	II	III	IV	V	VI	VII	VIII
3a	+0.98	+1.33	−0.49	−1.07	−1.54	−1.67	−2.08	−2.09	−2.44	−2.90
4	+0.97	+1.32	−1.51	−2.03	−2.49					
1a			−0.47	−1.06	−1.68	−2.15	−2.86			

To shed further light into this surprising observation, a digital simulation of the CV curve of Fig. 1(b) was carried out on the basis of the hypothesis that the third reduction of **4** is followed by a reversible dimerization process. The overall mechanism is outlined in Scheme 2.

A very good agreement is obtained with the experimental curve. The values for the direct and inverse reaction, which are coupled with the redox process III of **4**, are $k_f = 8 \times 10^5$ M^{-1} s^{-1}; $k_b = 0.5$ s^{-1}. On the other hand, the $E_{1/2}$ values used for the new redox couples I* and II* relative to the dimeric species are −1.43 and −1.80 V, respectively (see Fig. 1(c)).

The three reduction processes, observed for model **4**, correspond to peaks III, V and VII in dyad **3a** and they are likely due to the reduction of the porphyrin ring. Indeed, the first two reduction processes of the porphyrin ring compare rather well with the values reported for an analogous compound [12–14]. However, only the first two processes are reported in the literature, probably owing to a different available potential window, which was narrower than in the current work. Therefore, the dimerization process was not observed.

Perhaps not surprisingly, an analogous greater stability, this time, for the oxidized porphyrin, is also observed in the anodic region for **3a** with respect to **4**. Fig. 2(a) shows the CV curve, obtained under the conditions of Fig. 1(a), where along with the first four reduction processes in the cathodic region, two one-electron reversible oxidations, denoted as A and B, are observed in the anodic region. The corresponding $E_{1/2}$ values are reported in Table 1. Substantially different is the anodic CV pattern for **4** (Fig. 2(b)). Only the first oxidation step is fully reversible, while peak B is irreversible chemically. The irreversibility is evidenced by: (i) an i_{pc}:i_{pa} ratio lower than unity and (ii) the appearance of a novel and irreversible reduction peak C (0.23 V), in the reverse scan. This latter is not observed upon reversing the scan immediately after reaching the potential of peak A.

In line with an EC mechanism, increasing the scan rate leads to an increase in the reversibility of peak B and, accordingly, brings about the decrease and eventually the disappearance of peak C. The fact that the CV pattern is concentration independent suggests that the chemical reaction, following the second oxidation of **4**, is first order with respect to the porphyrin moiety. The digital simulation (Fig. 2(c)) of the CV curves is based on the mechanism summarized in Scheme 2 and resembles the experimental data nicely. Furthermore, the simulation provides the rate constants of the chemical follow-up processes as well as the $E_{1/2}$ value for process C. In particular, the rate constants are $k_1 = 4$ s^{-1} and $k_2 = 100$ s^{-1} and the redox potential for ($*\mathbf{4}^{2+}$/$*\mathbf{4}^{+}$) couple is 0.22 V (Scheme 3).

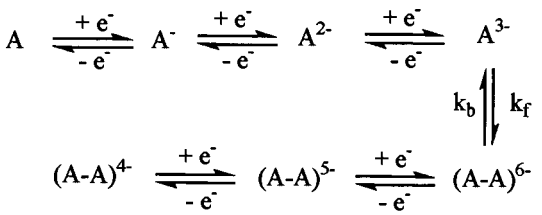

Scheme 2. Mechanism used in the digital simulation presented in Fig. 1(c). Species A represents the model compound **4**.

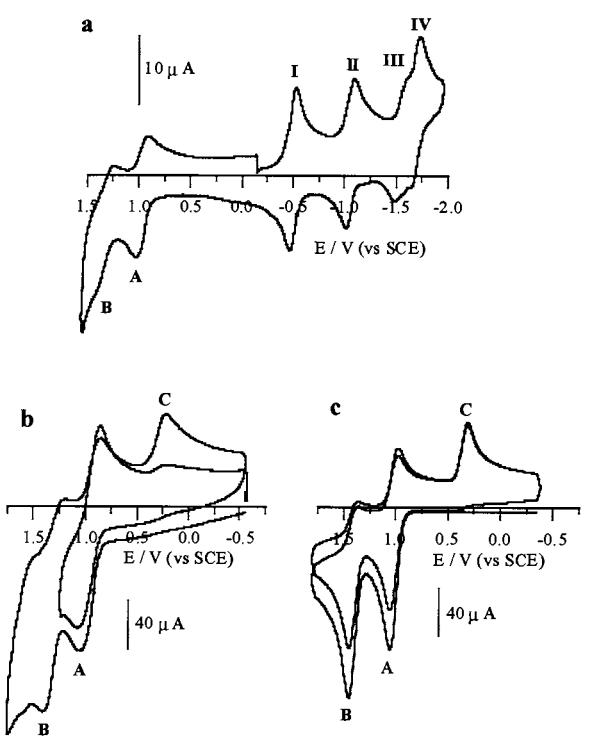

Fig. 2. CV curves at −60°C of a 0.4 mM TBAH–THF solution of (a) dyad **3a** and (b) model **4**. Working electrode: Pt wire (0.15 cm^2); $v = 0.5$ V s^{-1}. (c) Digital simulation in the conditions of (b).

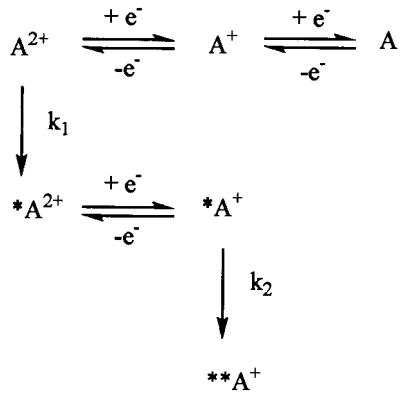

Scheme 3. Mechanism used in the digital simulation presented in Fig. 2(c). Species A represents the model compound **4**.

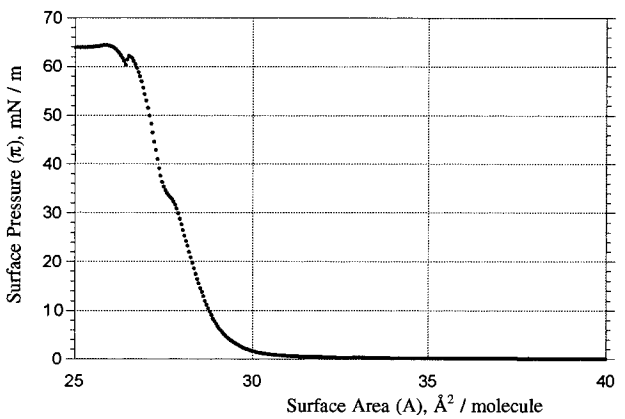

Fig. 3. Isotherm for the 1:20 molar mixture of **3b** and arachidic acid, respectively. Spreading solvent: chloroform. $T = 20°C$

The CO axial ligand is known to shift the Ru centered oxidation to very positive potentials [12,13]. Therefore, the two oxidation processes observed in **4** and **3a** are centered on the porphyrin ring. Moreover, the chemical irreversibility, which is associated with the second oxidation of **4**, is reminiscent of the behavior of a ZnTPP linked to a pyridine ligand [15–17]. In analogy to the Zn–porphyrin, the chemical reaction coupled with peak B can be associated with the formation of a β-substituted isoporphyrin, reduced in correspondence of peak C.

2.3. Langmuir–Blodgett films

For the present investigation, chloroform was chosen as the spreading solvent, since (i) aggregation phenomena; and (ii) solvent-related effects complicate interpretation of surface pressure–area isotherms. In fact, it has been reported that aromatic solvents often remain trapped in spread films. This, in fact, indicates a probable complexation of the solvent molecules by the fullerenes moieties [18–25].

Surface pressure (Π) versus surface area (A) isotherms of **3b** from chloroform spreading solutions (concentrations in the range of 10^{-4}–10^{-6} M) were registered. The structure of **3b** does not provide the adequate hydrophobic–hydrophilic balance to ensure the formation of stable, pure Langmuir monolayers at the air | water interface. This conclusion stems from the limiting area per molecule (i.e. 25 Å^2 molecule^{-1}), extracted from the steepest portion of the Langmuir isotherm through extrapolation to zero pressure, which contradicts the formation of a monolayer. Actually, the significantly reduced value suggests that the floating film of pure **3b** consists of more than a single monolayer in thickness. Therefore, during the compression cycle, the floating layer is assumed to be inhomogeneous and patchy as reported for a series of strongly hydrophobic substances [18–26].

To prepare condensed layers, a single molecule in thickness, and also with the objective of separating the dyad molecules from each other, we pursued the strategy of preparing floating films from a mixture of an amphiphilic molecule and **3b**. In this light, a 1:20 molar mixture of **3b** and arachidic acid in chloroform was used. The corresponding isotherm is illustrated in Fig. 3 and represents triplicate runs that gave identical results. The surface pressure (Π) versus surface area (A) isotherm consists of three distinct branches with quite different slopes. The first branch extends from $\Pi = 0$ to $\Pi = 30$ mN m^{-1}, which corresponds to an area per molecule of arachidic acid of nearly 29 Å^2 molecule^{-1} [27–29]. The second part of the plot, exhibiting a minor slope, covers the range between $\Pi = 30$ mN m^{-1} and about $\Pi = 35$ mN m^{-1}. Finally, the third region starts around $\Pi = 35$ mN m^{-1} and continues to the collapse pressure of the floating film. The latter gives rise to a limiting area of about 27 Å^2 molecule^{-1}.

This characteristic behavior is reproducible consistently and each of these distinct regions is probably characterized by different packing of molecules. Actually, both limiting values are near the value of the limiting area of cadmium arachidate monolayers. Therefore, our study suggests that at high surface pressures, the dyad molecules are gradually squeezed out of the acid monolayer (e.g. during the part as far as 30 mN m^{-1}). Between 30 and 35 mN m^{-1}, the slower variation in the surface pressure indicates a change in the arrangement of the dyad molecules within the hydrophobic environment (i.e. the hydrocarbon tails of the acid). Then, when $\Pi > 35$ mN m^{-1}, the dyad molecules are virtually on top of the hydrophobic arachidic acid layer.

Floating layers prepared from **3b** and arachidic acid were transferred to solid substrates (hydrophobic quartz and glass, silicon) by the LB technique. In the case of quartz substrates, the transfer was monitored by absorption spectrophotometry. Fig. 4 shows that the plot of absorbance at 340 nm versus the number of transferred layers is linear, which substantiates the

quality of the LB films formed. The absorption at 340 nm is mainly due to the dyad. In fact, the spectrum of cadmium arachidate onto quartz shows an insignificant absorption. After this, we conclude that (i) the deposition of the film is reproducible; (ii) a constant amount of **3b** is picked up at each up- and down-stroke; and (iii) the molecular environment of **3b** does not vary during the deposition. The transfer was of Y-type up to at least 160 layers on all substrates. The deposition ratio is a further clue to the quality of the multilayer, since it is always close to unity for both withdrawing and lowering the substrate through the floating film onto water.

Moreover, the average thickness, of 448 ± 20 nm, was measured by a Tencor computerized surface profiler (Alpha-Step 200) after the deposition of a thin gold layer, of known thickness, onto both a clean region of the quartz substrate and the LB film. The thickness of a pure cadmium arachidate monolayer onto hydrophobic quartz is reported to be 27 Å [30–32]. Thus, a multilayer 160 layers thick should therefore be 432 nm in thickness. The experimental value of 448 ± 20 nm is in excellent agreement with the theoretical one and is consistent with a uniform dispersion of **3b** molecules in the cadmium arachidate matrix.

2.4. Photophysical characterization

Light irradiation (532 nm) of solutions of dyad **3a** leads, analogously to the reference metalloporphyrin (**2**), to the local excitation of the porphyrin chromophore. It should be noted that the presence of the ruthenium leads to a very rapid intersystem crossing (> 35 ps), starting from the porphyrin singlet excited state ^{1}*(π–π*)RuTPP to the corresponding triplet excited state ^{3}*(π–π*)RuTPP (1.73 eV) [33]. In solution, dyad **3a** shows a solvent dependent deactivation of the ruthenium porphyrin triplet excited state. In particular, in non-polar solvents, such as toluene, a triplet–triplet energy transfer mechanism governs the photophysics of dyad **3a**, yielding almost quantitatively the fullerene triplet (1.5 eV). An endothermic intramolecular electron transfer to the high-lying charge-separated state was not observed. As a consequence of lowering the energy of the charge-separated state, for example, in more polar solvents (e.g. THF or benzonitrile) the electron transfer, evolving from the photoexcited metalloporphyrin (donor) to the coordinatively attached fullerene ligand (acceptor), becomes exothermic. In fact, transient spectra reveal the rapid transformation of the ruthenium porphyrin triplet excited state into the charge-separated state, namely, $RuTPP^{\bullet+}$–$C_{60}^{\bullet-}$. Spectral evidence for the latter state stems from the ruthenium porphyrin π-radical cation (e.g. $RuTPP^{\bullet+}$) and the fullerene π-radical anion absorption (e.g. $C_{60}^{\bullet-}$) around 650 and 1010 nm, respectively. Further details on the emission and transient absorption spectroscopy, by means of picosecond- and nanosecond-resolved photolysis, are given elsewhere [4].

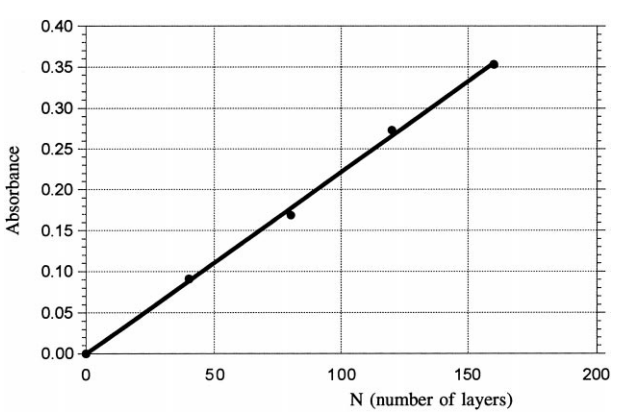

Fig. 4. Optical absorption at 340 nm vs. number of LB layers deposited onto hydrophobic quartz.

The promising intramolecular dynamics in solution led us to probe organized films (e.g. LB films) of dyad **3b** in photolytic experiments. In this context, we followed two different strategies: first, we probed simple LB films composed of homogeneously stacked dyad monolayers (e.g. 40 and 60 monolayers). The absorption cross section (~ 0.2) of the investigated films was sufficient at the excitation wavelength (532 nm) to guarantee the metalloporphyrins excitation. Surprisingly, no transient changes were observed throughout the UV–vis–NIR upon nanosecond-resolved flash photolysis. At first glance, this can be viewed as a parallel to closely packed fullerene films [34]. In the latter the fullerene singlet excited state is subject to a rapid decay (e.g. lifetime on the order of ~ 2 ps). The density dependence of the relaxation process has been interpreted in terms of a fast depopulation of the singlet excited state via singlet–singlet annihilation. In conclusion, a rapid triplet–triplet annihilation governs the fate of the excited metalloporphyrin in organized films of dyad **3b**.

To circumvent the annihilation problem, we moved to the second strategy, namely the study of films which were deposited from mixed dyad **3b**/AA monolayers. In these intercalated LB films, the dyad molecules are believed to be sufficiently separated from each other, thus ruling out their electronic communication. Now, intramolecular electron transfer or energy transfer events from the ^{3}*(π–π*)RuTPP should prevail over the undesired triplet–triplet annihilation processes. Indeed, recording differential absorption changes, upon laser photolysis, throughout the UV–vis–NIR region led to characteristic changes. In principle, this substantiates the concept of employing mixed dyad **3b**/AA monolayers. Characterization of the intermediate was performed via the differential absorption spectrum in the NIR region. In the latter region the product exhibits the

fingerprint of the fullerene π-radical anion, namely, a maximum around 1010 nm. From the decay kinetics of the π-radical anion absorption we were able to deduce the lifetime of the charge-separated radical pair. In particular, a lifetime of ~ 2.2 μs indicates quite a significant stabilization of the radical pair. At the moment we cannot assign if the stabilization is gained via a possible electron migration/hopping mechanism between different dyad molecules or via complex dissociation as, for example, noted in condensed media (e.g. benzonitrile). Considering, however, the constrained medium, electron migration/hopping appears more feasible as a responsible mechanism.

3. Conclusions

The synthesis is reported of an amphiphilic dyad, based on metal complexation of a ruthenium tetraphenyl porphyrin by a fullerene derivative functionalized with a pyridine ring and a hydrophilic chain. Cyclic voltammetry study shows that several electron transfers occur during the scan. A greater stability of the dyad in terms of reduced and oxidized species is observed. The dyad can be spread on a quartz slide as a 1:20 mixture with arachidic acid. Photophysical studies, performed by transient absorption spectrophotometry demonstrate that electron transfer occurs in the solid film with a lifetime of ~ 2.2 μs.

4. Experimental

4.1. General

^{1}H and ^{13}C spectra were recorded on a Varian Gemini 200 spectrometer. Chemical shifts are given in parts per million (δ) relative to tetramethylsilane. UV–vis absorption spectra were obtained on a Jasco V550 UV–vis spectrophotometer. Electrospray mass spectra were taken on a PE SCIEX API-1 spectrometer. Voltammograms were recorded with a AMEL model 552 potentiostat or a custom-made fast potentiostat controlled by either a AMEL model 568 function generator or a ELCHEMA model FG-206F. Data acquisition was performed on a Nicolet model 3091 digital oscilloscope interfaced to a PC.

4.2. Materials

C_{60} was purchased from Bucky USA (99.5%). Fulleropyrrolidines (**1a**,**b**) were prepared according to published procedures [8,9]. Compound **2** was purchased from Aldrich and used without further purification. Arachidic acid was purchased from Fluka (BioChemica) and was recrystallized from chloroform. All solvents were distilled prior to use.

4.3. Preparation of complex *3b*

A solution of **2** (2.67 mg, 3.6×10^{-3} mmol) in chloroform (2 ml) was added to **1b** (3.55 mg, 3.6×10^{-3} mmol in 2 ml of chloroform). The mixture was stirred at room temperature (r.t.) for 5 min. The solvent was removed, the residue was dissolved in CH_2Cl_2 and precipitated by addition of methanol.

$C_{119}H_{50}N_6O_4Ru$ (M_W, 1728.83), yield 99% (6.22 mg, 3.6×10^{-3} mmol). ^{1}H-NMR (200 MHz, $CDCl_3$): δ 8.53 (m, 8H), 8.17 (m, 4H), 7.85 (m, 4H), 7.66 (m, 8H), 7.55 (m, 4H), 5.70 (m, 2H), 4.71 (d, $J = 9.9$ Hz, 1H), 4.05 (s, 1H), 3.77 (d, $J = 9.9$ Hz, 1H), 3.51–3.36 (m, 12H), 3.23 (s, 3H), 1.58 (m, 2H). ^{13}C-NMR (50 MHz, $CDCl_3$): δ 179.7, 155.4, 153.1, 151.3, 150.7, 147.2, 147.2, 146.2, 146.2, 146.1, 146.0, 145.9, 145.8, 145.4, 145.3, 145.2, 145.1, 145.1, 145.0, 144.5, 144.3, 144.2, 143.6, 143.5, 143.5, 143.4, 143.3, 143.1, 143.1, 142.8, 142.6, 142.6, 142.5, 142.4, 142.0, 141.9, 141.9, 141.8, 141.5, 141.5, 141.2, 141.2, 140.9, 139.3, 139.2, 135.8, 135.7, 135.7, 135.1, 134.1, 134.0, 131.8, 127.2, 126.5, 126.1, 122.0, 121.6, 79.1, 74.5, 71.8, 70.5, 70.3, 69.6, 68.6, 66.8, 59.0, 51.2. ES MS (THF–MeOH 4:1): m/z 987. UV–vis (cyclohexane): λ_{max} (nm) 530, 409, 314, 255.

4.4. Cyclic voltammetry

The substrates and the supporting electrolyte Bu_4NPF_6 were added into a single-compartment airtight cell, which was then degassed and pumped to $1–2 \times 10^{-5}$ mbar. The dried solvent (THF, CH_3CN, or CH_3CN–CH_2Cl_2) was then transferred as a vapor directly into the cell from a Schlenck vessel in which it was stored under reduced pressure.

4.5. Langmuir–Blodgett film deposition

The concentrations of **3b** and arachidic acid in the spreading solution in chloroform were 1.4×10^{-4} and 2.8×10^{-3} M, respectively. The subphase was ultrapure water (resistivity greater than 18 MΩ cm) from a Millipore Elix3/MilliQ-Plus system, containing 3×10^{-4} M $CdCl_2$ and buffered with 10^{-5} M $KHCO_3$ to pH 5.8. It was thermostatted at 20°C by a Hake GH-D8 apparatus. Finally, LB films were prepared by using a KSV5000 System3 apparatus (850 cm^2).

In the Langmuir trough experiments, a 100 μl portion of the solution was carefully spread onto the subphase by a gas-tight syringe. After the solvent was evaporated (ca. 10 min), the floating film was compressed continuously at a speed of 5 mm min^{-1}. Surface pressure was simultaneously monitored by a Wilhelmy balance while getting an isotherm of the sample. The substrates (hydrophobic glass and quartz) were washed for 3 h with ethyl acetate using a Soxhlet extractor, dried in clean air and placed in contact with

hexamethyldisilazane vapors for 12 h. The films were then transferred onto the substrates by the usual vertical dipping method at the surface pressure of 25 mN m^{-1} and at a speed of 4 mm min^{-1} during the downstroke and 6 mm min^{-1} during the upstroke. Y-type deposition up to 160 layers was obtained onto hydrophobic quartz; the deposition ratio for both withdrawing and lowering the substrate through the floating film onto water was always in the range 1.00 ± 0.05.

Acknowledgements

This work was supported by MURST (cofin. ex 40%, prot. n. 9803194198_005), the University of Bologna (Funds for selected research topics), by CNR through the program 'Materiali Innovativi (legge 95/95)' and by the European Community (TMR program USEFULL, contract no. ERB FMRX-CT97-0126). Part of this work was supported by the Office of Basic Energy Sciences of the Department of Energy. This is document NDRL-4182 from the Notre Dame Radiation Laboratory.

References

[1] N. Armaroli, F. Diederich, L. Echegoyen, T. Habicher, L. Flamigni, G. Marconi, J.-F. Nierengarten, New J. Chem. (1999) 77.
[2] F. D'Souza, G.R. Deviprasad, M.S. Rahman, J.-P. Choi, Inorg. Chem. 38 (1999) 2157.
[3] T. Da Ros, M. Prato, D. Guldi, E. Alessio, M. Ruzzi, L. Pasimeni, Chem. Commun. (Cambridge) (1999) 635.
[4] T. Da Ros, M. Prato, D.M. Guldi, M. Ruzzi, L. Pasimeni (submitted).
[5] N. Martín, L. Sànchez, B. Llescas, I. Pérez, Chem. Rev. 98 (1998) 2527.
[6] M. Prato, J. Mater. Chem. 7 (1997) 1097.
[7] M. Prato, Top. Curr. Chem. 199 (1999) 173.
[8] M. Maggini, G. Scorrano, M. Prato, J. Am. Chem. Soc. 115 (1993) 9798.
[9] M. Prato, M. Maggini, Acc. Chem. Res. 31 (1998) 519.
[10] P. Wang, B. Chen, R.M. Metzger, T. Da Ros, M. Prato, J. Mater. Chem. 7 (1997) 2397.
[11] T. Da Ros, M. Prato, F. Novello, M. Maggini, E. Banfi, J. Org. Chem. 61 (1996) 9070.
[12] K. Funatsu, K. Kimura, T. Imamura, A. Ichimura, Y. Sasaki, Inorg. Chem. 36 (1997) 1625.
[13] D.F. Rillema, J.K. Nagle, L.F. Barringer, Jr., T.J. Meyer, J. Am. Chem. Soc. 103 (1981) 56.
[14] G.M. Brown, F.R. Hopf, J.A. Ferguson, T.J. Meyer, D.G. Whitten, J. Am. Chem. Soc. 95 (1973) 5939.
[15] F. D'Souza, Y.-Y. Hsieh, G.R. Deviprasad, Inorg. Chem. 35 (1996) 5747.
[16] L. El Kahef, M. El Meray, M. Gross, A. Giraudeau, J. Chem. Soc. Chem. Commun. (1986) 621.
[17] H.J. Shine, A.G. Padilla, S.-M. Wu, J. Org. Chem. 44 (1979) 4069.
[18] F. Diederich, J. Effing, U. Jonas, L. Jullien, T. Plesnivy, H. Ringsdorf, C. Thilgen, D. Weinstein, Angew. Chem. Int. Ed. Engl. 31 (1992) 1599.
[19] F. Diederich, U. Jonas, V. Gramlich, A. Herrmann, H. Ringsdorf, C. Thilgen, Helv. Chim. Acta 76 (1993) 2445.
[20] U. Jonas, F. Cardullo, P. Belik, F. Diederich, A. Gügel, E. Harth, A. Herrmann, L. Isaacs, K. Müllen, H. Ringsdorf, C. Thilgen, P. Uhlmann, A. Vasella, C.A.A. Waldraff, M. Walter, Chem. Eur. J. 1 (1995) 243.
[21] N.C. Maliszewskyi, P.A. Heiney, D.H. Jones, R.M. Strongin, M.A. Cichy, A.B. Smith, III, Langmuir 9 (1993) 1439.
[22] G. Williams, A. Soi, A. Hirsch, M.R. Bryce, M.C. Petty, Thin Solid Films 230 (1993) 71.
[23] G. Williams, A.G. Moore, M.R. Bryce, Y.M. Lvov, M.C. Petty, Synth. Met. 55–57 (1993) 2955.
[24] M. Maggini, L. Pasimeni, M. Prato, G. Scorrano, L. Valli, Langmuir 10 (1994) 4164.
[25] F. Cardullo, F. Diederich, L. Echegoyen, T. Habicher, N. Jayaraman, R. Leblanc, J. Stoddart, S. Wang, Langmuir 14 (1998) 1955.
[26] D.P. Arnold, D. Manno, G. Micocci, A. Serra, A. Tepore, L. Valli, Langmuir 13 (1997) 5951.
[27] Y.S. Obeng, A.J. Bard, J. Am. Chem. Soc. 113 (1991) 6279.
[28] C. Jehoulet, Y.S. Obeng, Y.-T. Kim, F. Zhou, A.J. Bard, J. Am. Chem. Soc. 114 (1992) 4237.
[29] G.G. Roberts, Langmuir–Blodgett Films, Plenum, New York, 1990.
[30] M.C. Petty, in: G.G. Roberts (Ed.), Langmuir–Blodgett Films, Plenum, New York, 1990.
[31] T. Onishi, A. Ishitani, H. Ishida, N. Yamamoto, H. Tsubomura, J. Phys. Chem. 82 (1978) 1989.
[32] J.F. Rabolt, F.C. Burns, N.E. Schlotter, J.D. Swalen, J. Electron. Spectrosc. Relat. Phenom. 30 (1983) 29.
[33] C.D. Tait, D. Holten, M.H. Barley, D. Dolphin, B.R. James, J. Am. Chem. Soc. 107 (1985) 1930.
[34] T.N. Thomas, R.A. Taylor, J.F. Ryan, D. Mihailovic, R. Zamboni, in: H. Kuzmany, J. Fink, M. Mehring, S. Roth (eds.), Electronic Properties of Fullerenes, Springer-Verlag, Berlin, 1993, p. 292.